Kinetics of $O_2(^1\Sigma_g^+)$ Reaction with H_2 and an Upper Limit for OH Production†

Ranajit K. Talukdar,*,#,‡ Edward J. Dunlea,#,‡,§ Steven S. Brown,#,‡ John S. Daniel,# and A. R. Ravishankara#,‡,§

Aeronomy Laboratory, NOAA, R/AL2, 325 Broadway, Boulder, Colorado 80305, and CIRES, University of Colorado at Boulder, Boulder, Colorado 80309

Received: March 1, 2002; In Final Form: May 30, 2002

The rate coefficients for the removal of $O_2(^1\Sigma_g^+)$ (from now on referred to as $O_2(^1\Sigma)$) by H_2 were measured between 209 and 373 K by generating $O_2(^1\Sigma)$ via pulsed laser excitation near 762 nm. The rate coefficient was determined to be $k_1 = (6.8 \pm 1.2) \times 10^{-12} \exp[-(590 \pm 52)/T]$ cm^3 molecule^{-1} s^{-1}. Reaction of $O_2(^1\Sigma)$ with O_3 yielded $O(^3P)$, which was detected by vacuum ultraviolet (VUV)-resonance fluorescence. $O_2(^1\Sigma)$ was also prepared by the interaction of $O(^1D)$ with O_2. In separate experiments, the yield for OH from the title reaction was measured to be $<4 \times 10^{-5}$ at 298 and 209 K. This upper limit was used in a one-dimensional atmospheric model to show that the contribution of this reaction to the total OH production in the atmosphere is minimal under most conditions.

Introduction

Toumi[1] and Siskind et al.[2] have proposed that the reaction of $O_2(^1\Sigma)$ with H_2 may lead to the production of OH and that this process may be important in the Earth's atmosphere. Below roughly 25 km, $O_2(^1\Sigma)$ is mainly produced by absorption of 762 nm light by ground-state oxygen, $O_2(^3\Sigma)$. In the 30−60 km region, the quenching of $O(^1D)$ by ground-state O_2 is the important source of $O_2(^1\Sigma)$. The majority of $O_2(^1\Sigma)$ is quenched to either $O_2(^1\Delta)$ or $O_2(^3\Sigma)$ by N_2 and H_2O in the atmosphere. Yet, because the rate coefficient for the removal of $O_2(^1\Sigma)$ by N_2 is small compared to that by H_2, a small fraction of $O_2(^1\Sigma)$ ($\sim 1 \times 10^{-4}$) is quenched by or reacts with H_2 in the atmosphere. The primary interaction of $O_2(^1\Sigma)$ with H_2 is quenching,[3−5]

$$O_2(^1\Sigma) + H_2 \rightarrow O_2(^1\Delta) + H_2 \ (v \le 1) \quad \text{or} \quad O_2(^3\Sigma) + H_2 \ (v \le 3) \qquad k_{1a} \quad (1a)$$

However, Toumi and Siskind et al. pointed out that even a small yield of OH in this reaction,

$$O_2(^1\Sigma) + H_2 \rightarrow 2OH \qquad \Delta_r H°(298) = -18.9 \text{ kcal mol}^{-1} \qquad k_{1b} \quad (1b)$$

could be significant in the atmosphere. For example, at high solar zenith angles (>85°), the rate of ultraviolet photolysis of ozone to give $O(^1D)$ decreases relative to the photoexcitation of O_2. Under these conditions in the upper troposphere, a 1−4% yield of OH in reaction 1 could produce as much OH as the reaction of $O(^1D)$ with H_2O. The latter source is currently believed to be the major source of atmospheric OH. In addition to reaction channels 1a and 1b, another exothermic channel (1c) is also possible

$$O_2(^1\Sigma) + H_2 \rightarrow O(^3P) + H_2O \qquad \Delta_r H°(298) = -35.7 \text{ kcal mol}^{-1} \qquad k_{1c} \quad (1c)$$

However, this pathway has been shown to be negligible.[6]

The rate coefficient for the removal of $O_2(^1\Sigma)$ in reaction 1, $k_1 = k_{1a} + k_{1b}$, has been measured previously.[3,5,7−12] The obtained values at 298 K differ by almost a factor of 2.[7−10] The temperature dependence of k_1 has been measured by four of these studies and the agreement between those results is reasonable. However, because of the discrepancies among the different studies, a remeasurement of k_1 as a function of temperature would be beneficial.

In this paper, we report the temperature dependence of k_1, the measured upper limits for the branching ratio for the production of OH in reaction 1, and the atmospheric implications of our data deduced by using model calculations.

Experiments

The experimental section consists of several subsections describing different aspects of this study. To determine the yield of OH in reaction 1, it was essential to (a) prepare known concentrations of $O_2(^1\Sigma)$, (b) determine the total rate coefficient for the removal of $O_2(^1\Sigma)$ by reaction with H_2, and (c) calibrate the quantitative response of the OH−laser-induced fluorescence (LIF) system for determination of a limit on the branching ratio for reaction 1b.

1. Apparatus and Methods. A schematic of the experimental setup is shown in Figure 1. Two different methods were employed to prepare known concentrations of $O_2(^1\Sigma)$: (a) ground-state oxygen, $O_2(^3\Sigma)$, was excited to $O_2(^1\Sigma)$ by collision with $O(^1D)$ produced by the photolysis of O_3 at 248 nm; (b) O_2 was directly excited by tunable radiation near 762 nm from a dye laser pumped by 532 nm (second harmonic) output from a Nd:YAG laser. Preparation of a large, known concentration of

† Part of the special issue "Donald Setser Festschrift".

* To whom correspondence should be addressed at NOAA, R/AL2, 325 Broadway, Boulder, CO 80305.

Aeronomy Laboratory, NOAA.

‡ CIRES, University of Colorado at Boulder.

§ Also associated with Department of Chemistry and Biochemistry, University of Colorado, Boulder, CO 80309.

10.1021/jp020589j CCC: $22.00
Published on Web 07/17/2002

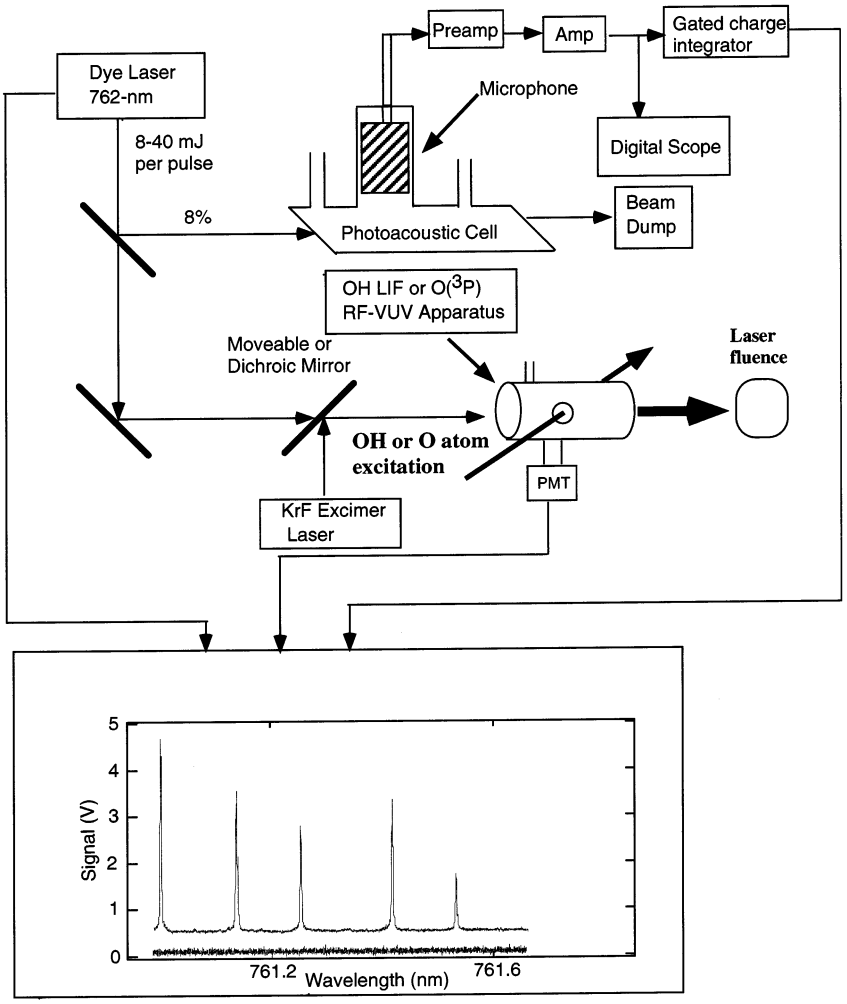

Figure 1. Schematic of the experimental set up used to measure k_1 and the yield of OH in reaction 1.

$O_2(^1\Sigma)$ via excitation from the ground state requires optimum overlap between the dye-laser output and the Doppler and collisionally broadened O_2 absorption lines. The dye-laser line width was reduced by using an intracavity air-spaced Etalon placed in a box filled with variable pressures of SF_6. The pressure of SF_6 in the box was varied to tune the laser wavelength. Approximately 8% of the dye-laser output was diverted into a photoacoustic cell containing 10 Torr of O_2. Maximization of the photoacoustic signal ensured optimum overlap between the dye-laser frequency and the O_2 transition. The remaining portion of the 762-nm laser beam and the 248-nm laser beam were aligned and collimated through a set of apertures to propagate along the same path in the reactor. Only one mirror needed to be repositioned (using a kinematic mount to ensure reproducibility) to switch between the two excitation laser beams; this arrangement was used in both OH and $O(^3P)$ detection apparatuses. In some experiments, the 762 and the 248-nm laser beams were combined using a beam combining mirror and copropagated through the same set of apertures.

2. Photoacoustic Spectroscopy. A glass cell (18 cm long with an inner diameter of 2.2 cm) containing a sensitive microphone (a piezoelectric transducer) and equipped with quartz windows mounted at Brewster's angle was used to tune the dye laser onto an O_2 transition. Two variable apertures were placed at the entrance and exit of the cell to reduce the scattered laser light. The signal from the microphone was fed to the preamplifier through a BNC vacuum feed-through. The output of the preamplifier was further processed with a conditioning amplifier tuned to the resonant frequency of the cell (26 kHz) and was fed to a gated integrator for averaging.

The photoacoustic signal and the output of the transducer that monitored the pressure of SF_6 in the Etalon box were fed to an eight-channel A-to-D converter; the digitized signals from the converter were recorded simultaneously on a personal computer. The photoacoustic spectra between 759 and 768 nm of 10 Torr of O_2 at 296 K were recorded via several successive SF_6 pressure scans, each covering a 0.7 nm segment; the segments overlapped each other. The laser line width was derived from these spectra as described in the appendix (Appendix A). The absorption line width of O_2 at a pressure of 10 Torr in the photoacoustic cell was narrower than that in the reactor with 150 Torr of O_2. The photoacoustic signal was merely used to ensure that the 762-nm laser was indeed on the O_2 absorption peak.

3. $O(^3P)$ Detection. The temporal profiles of $O(^3P)$ were used to monitor the kinetics of $O_2(^1\Sigma)$ and to quantify $[O_2(^1\Sigma)]_0$. $O(^3P)$ was detected by vacuum ultraviolet (VUV) atomic resonance fluorescence. The schematic of the experiment is shown in Figure 1. The VUV-resonance fluorescence detection of $O(^3P)$ is routinely done in this laboratory; the details are given elsewhere.[13,14]

Briefly, a jacketed Pyrex cell was maintained at a constant temperature by flowing cooled methanol or heated ethylene glycol from a thermostated bath. The temperature in the reaction

zone, defined by the intersection of the photolysis and VUV resonance lamp beams, was measured by a retractable thermocouple. The measured temperature was constant to within ±1 K and known to better than 0.5 K. Gas mixtures containing O_3/ultrahigh purity (UHP) O_2, H_2, and He were flowed through the reaction cell. All of the gas flow rates, except that of O_3, were measured by calibrated electronic mass flow meters. Ozone was flowed from a 12-L bulb containing a 2% mixture of O_3 in He. The concentration of ozone in the reaction mixture flowing through the reactor was measured by 253.6 nm (Hg pen ray lamp) absorption in a 100 cm cell located just upstream of the reactor. The ozone concentration ranged between 1×10^{13} and 15×10^{13} molecule cm^{-3}. The O_2 pressure was 3−13 Torr, while the total pressure was 12−70 Torr. The linear gas flow velocity in the reactor was between 10 and 20 cm s^{-1}.

To determine k_1, $O_2(^1\Sigma)$ was generated by direct 762-nm excitation of ground-state O_2. The temporal profiles of $O(^3P)$, produced by the reaction of $O_2(^1\Sigma)$ with O_3, were measured at different H_2 concentration in mixtures of O_3, O_2, H_2, and He. The detection limit for $O(^3P)$ for a signal-to-noise ratio of unity for 1 s integration time was determined to be 2×10^8 atom cm^{-3} in 15−80 Torr of He and 6×10^8 atom cm^{-3} in a mixture of 5 Torr of O_2/15−80 Torr of He.

4. OH Detection. The experimental setup is shown in Figure 1. The details of the apparatus, data acquisition methodology, and data analysis are given elsewhere.[15,16] Briefly, a 150-cm^3 Pyrex jacketed cell was maintained at constant temperatures as described above. The hydroxyl radical was detected by laser-induced fluorescence (LIF) pumped by a pulsed laser. The temporal profiles of OH were measured by varying the time delay between the photolysis and probe lasers. Experiments were conducted at 298 and 209 K. The gas mixtures containing H_2 and O_2 in He, with known concentrations of O_3 or H_2O_2 or both, were flowed through the reaction cell. The O_3 concentration was measured via UV absorption, as described earlier. The concentrations and pressures of various reactants and buffer gases used were as follows: $[H_2] = (0.1-53) \times 10^{16}$ molecule cm^{-3}, $[O_2] = (4-7) \times 10^{18}$ molecule cm^{-3}, $[O_3] = (1-2) \times 10^{14}$ molecule cm^{-3}, $[H_2O_2] = (3-5) \times 10^{14}$ molecule cm^{-3}, and total pressure = 150−250 Torr.

Photolysis of an $O_3/O_2/H_2$ mixture at 248 nm produced $O(^1D)$; $O(^1D)$ was quenched by O_2 to generate $O_2(^1\Sigma)$ in less than 100 ns. A small quantifiable fraction (<1%) of $O(^1D)$ also reacted with H_2 to make OH, which acted as an internal calibration for OH. When $O_2(^1\Sigma)$ was generated by 762-nm excitation, OH was not produced via photolysis. Therefore, we needed to calibrate the OH signal to determine the sensitivity of the apparatus to detect OH under the conditions employed. We did back-to-back experiments in which we first produced a known concentration of OH via the 248 nm photolysis of a mixture of O_3 and H_2 and then excited O_2 at 762 nm to determine how much OH was produced by reaction 1. The fluences of the two laser beams were measured at the exit of the reactor with a calibrated power meter and were in the range 1−5 mJ cm^{-2} $pulse^{-1}$ and 12−30 mJ cm^{-2} $pulse^{-1}$ for 248 and 762 nm beams, respectively. According to the manufacturer's specification, the response of the power meter was the same (within 10%) between 193 and 810 nm. The linearity of the response of the power meter was checked against another power meter that had been previously calibrated at 248 nm by calorimetric method (Marla Dowell/NIST, private communication).

To measure the OH yield from reaction 1, a mixture of $O_3/O_2/H_2$ was photolyzed at 248 nm and the signal from OH was obtained. Then, the 248 nm laser was replaced by the 762-nm dye laser, and O_3 was taken out of the reactor (to prevent the loss of $O_2(^1\Sigma)$ via its reaction with O_3). The dye laser was pressure tuned to individual rotational lines of the $O_2(^1\Sigma) \leftarrow O_2(^3\Sigma)$ (0-0) transition. The OH signal, the photoacoustic signal, and the dye-laser wavelength (as measured by the pressure in the grating box) were recorded simultaneously. The dye-laser wavelength was scanned rapidly between absorption lines but was slowed to scan across an absorption feature. In the middle of the scan, a measured concentration of O_3 was added to the reactor and was photolyzed by 248 nm to calibrate the OH signal under the conditions of the experiment. Then, ozone was turned off and switched back to 762 nm, and the scan was continued.

5. Material. Ozone was prepared by passing O_2 through a commercial ozonizer and stored over silica gel at 195 K. It was degassed at 77 K before use. UHP-grade helium (99.9995%) was obtained from US Welding. UHP-grade O_2 (99.9995%) and H_2 (99.999%) were supplied by Scott Specialty gases. H_2O_2 was purified by prolonged (∼10 days) bubbling of helium through it. This procedure produced >97% pure H_2O_2 with the major impurity being H_2O.

Results and Discussions

For ease of presentation, we will describe and discuss the results from different experiments separately. First we will describe our determination of the initial concentration of $O_2(^1\Sigma)$ generated by 762 nm excitation of O_2. Second, we will describe our measurement of the total rate coefficient for the removal of $O_2(^1\Sigma)$ by H_2 and compare it with previous measurements. Third, we describe the results of our attempt to ascertain the yield of OH in reaction 1.

1. Efficiency of $[O_2(^1\Sigma)]$ Production in 762-nm Excitation of O_2. The initial concentration of $O_2(^1\Sigma)$, $[O_2(^1\Sigma)]_0$, is one of the key parameters needed to calculate the branching ratio for OH production in reaction 1. We calculated $[O_2(^1\Sigma)]_0$ from the measured laser fluence, the laser line width, the absorption cross sections for the O_2 lines, and the known $[O_2]$. The details of this calculation are given in Appendix A. In addition, we experimentally determined the $[O_2(^1\Sigma)]_0$ produced by the 762 nm laser excitation as described below.

A mixture of O_3 and O_2 flowing through the reactor was photolyzed at 248 nm. The reactions that occur in such a mixture upon photolysis are listed in Table 1. (Table 1 also lists the reactions involving H_2 for later reference). The $O(^1D)$ produced via ozone photolysis (reactions 2 and 3) reacted with O_2 (5 Torr partial pressure) within 1 μs (>99.8% completion) to generate $O(^3P)$ and $O_2(^1\Sigma)$; $O_2(^1\Sigma)$ subsequently reacted with O_3 (reaction 6a) to generate $O(^3P)$. Thus, for each ozone molecule that was photolyzed at 248 nm, roughly two $O(^3P)$ atoms were produced. By measuring the temporal profile of $O(^3P)$, we could separate the $O(^3P)$ produced via reaction 6a from that generated from a combination of the photolysis of O_3 and quenching of $O(^1D)$ (reactions 2−4). Thus, the initial concentration of $O_2(^1\Sigma)$ could be calculated from the measured laser fluence and ozone concentration and the known quantum yield for $O(^1D)$ production and the yield of $O_2(^1\Sigma)$ in the quenching of $O(^1D)$ by O_2.

In back-to-back experiments, the above mixture was photolyzed first at 248-nm and then excited at 762-nm (tuned to an O_2 transition). The two laser beams had exactly the same beam diameters and traveled through the same volume in the reactor. The 762-nm dye laser was tuned to the peak of an O_2 transition; this was determined by monitoring the photoacoustic signal as well as the $O(^3P)$ signal from reaction 6. The observed temporal profiles of $O(^3P)$ in 248- and 762-nm excitation of an $O_3/O_2/He$ mixture are shown in Figure 2.

TABLE 1: List of Reactions that Occur upon 248 nm Photolysis of O_3 in O_2 and H_2

reaction number	reactions
1a	$O_2(^1\Sigma) + H_2 \rightarrow O_2 + H_2$
1b	$O_2(^1\Sigma) + H_2 \rightarrow 2OH$
1c	$O_2(^1\Sigma) + H_2 \rightarrow O(^3P) + H_2O$
2	$O_3 \xrightarrow{248\ nm} O(^1D) + O_2(^1\Delta)$
3	$O_3 \xrightarrow{248\ nm} O(^3P) + O_2(^3\Sigma)$
4	$O(^1D) + O_2 \rightarrow O(^3P) + O_2(^1\Sigma)$
5	$O(^1D) + X \rightarrow$ loss of $O(^1D)$ via processes not producing $O(^3P)$
6a	$O_2(^1\Sigma) + O_3 \rightarrow O(^3P) + 2O_2$, Φ_6
6b	$O_2(^1\Sigma) + O_3 \rightarrow$ loss of $O_2(^1\Sigma)$ not giving $O(^3P)$
7	$O_2(^1\Sigma) \rightarrow k_7$, diffusion loss and loss via reaction with O_2
8	$O(^3P) \rightarrow k_8$, diffusion loss and loss via reaction with O_2
9	$O(^1D) + O_3 \rightarrow O(^3P) + {}^3/_2O_2$
10	$O(^1D) + H_2 \rightarrow OH + H$
11	$OH + H_2 \rightarrow H_2O + H$
12	$OH + O_3 \rightarrow HO_2 + O_2$

The possible loss of $O(^1D)$ via its reaction with ozone is very small compared to its removal via quenching by O_2. Therefore, it is neglected in the analysis. The yield of $O_2(^1\Sigma)$ in reaction 4 is assumed to be unity, an assumption that is good to 20%. The yield of $O(^3P)$ in reaction 6 is denoted by Φ_6. The quantum yield for $O(^1D)$ in ozone photolysis, reaction 2, is 0.9.

Under the conditions in which reactions 5, 7, and 8 are negligible compared to other processes in this system, the maximum $O(^3P)$ produced is given by

$$[O(^3P)]_{max}^{248} = ([O(^1D)]_0 + [O(^3P)]_0) + \Phi_6[O(^1D)]_0 \quad (I)$$

where the first term in the parenthesis is the sum of $O(^1D)$ and $O(^3P)$ produced in ozone photolysis and the second term is the $O(^3P)$ produced from the reaction of $O_2(^1\Sigma)$ with ozone. Equation I can be rewritten as

$$[O(^3P)]_{max}^{248} = ([O_3]E_{248}\sigma_{248}) + \Phi_6(0.9[O_3]E_{248}\sigma_{248}) \quad (II)$$

where the first term is the amount of O_3 photolyzed (and thus equal to the sum of $O(^1D)$ and $O(^3P)$ produced) and the second term is the $O(^3P)$ produced from reaction 6. E_{248} is the 248-nm laser fluence in units of mJ cm^{-2} pulse^{-1} and σ_{248} is the absorption cross section of ozone in units of cm^2 molecule^{-1} at 248 nm. Note that the quantity in the second parenthesis is also the initial concentration of $O(^1D)$ produced in the photolysis of ozone.

When the same mixture is excited by 762 nm radiation, the concentration of $O(^3P)$ produced is given by

$$[O(^3P)]_{max}^{762} = \Phi_6([O_2]E_{762}P_E) \quad (III)$$

where P_E is the probability for excitation of O_2 from the ground $^3\Sigma$ state to the excited $^1\Sigma$ state and E_{762} is the 762-nm laser fluence in units of mJ cm^{-2} pulse^{-1}. P_E is defined as the fraction of molecules excited for the laser fluence of 1 mJ cm^{-2} pulse^{-1}. This includes line strength and line shape functions of O_2 lines (Doppler and collisional broadening) and the line shape function of the 762-nm laser beam. We calculated P_E by comparing eqs II and III and using the $O(^3P)$ signals from the back-to-back experiments (Figure 2).

In reality, the temporal profiles of $O(^3P)$ were analyzed to calculate the maximum amount of $O(^3P)$ that was produced and thus take into account the small contributions of reactions 5, 7, and 8 to the $O(^3P)$ profile. The temporal profile of $O(^3P)$ is given by

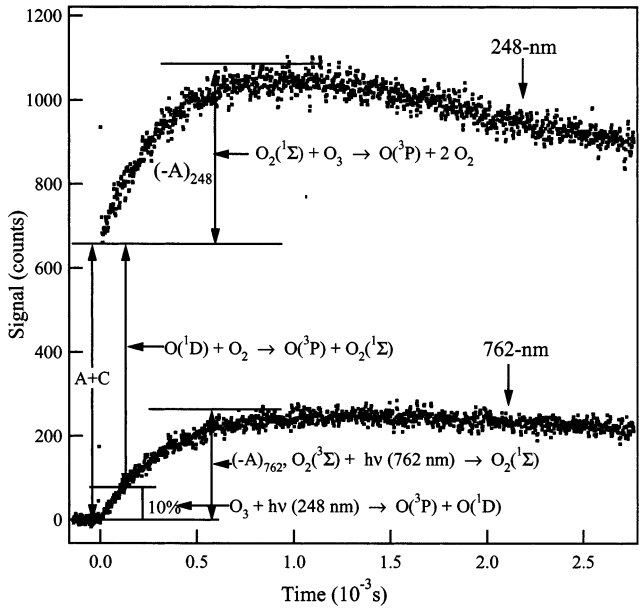

Figure 2. Temporal profiles of $O(^3P)$ in O_3 and O_2 following 248 nm photolysis (upper curve) and 762 nm (lower curve) laser excitation. The figure illustrates the contributions of different processes to the $O(^3P)$ temporal profile measured following the photolysis of ozone (1.11×10^{14} molecule cm^{-3}) at 248 nm in the presence of excess O_2 (1.36×10^{17} molecule cm^{-3}) at a total pressure of 20 Torr.

$$A\exp(-Bt) + C\exp(-Dt) \quad (IV)$$

where

$$A = -(k_{6a}[O_3][O_2(^1\Sigma)]_0)/(k_6[O_3] + k_7 - k_8) \quad (V)$$

$$B = k_6[O_3] + k_7 \quad (VI)$$

$$C = [O(^3P)]_0 - A, \quad D = k_8 \quad (VII)$$

In the case of 762-nm laser excitation of O_2 to produce $O_2(^1\Sigma)$, $A + C = [O(^3P)]_0$. The $O(^3P)$ produced by the photolysis of O_3 in the weakly absorbing Chappius band,[17,18] which was <1% of the total $O(^3P)$ produced in reaction 6, was also included. The observed temporal profiles were fit to eq IV by using nonlinear least squares routines to obtain the values of A and C parameters. The first and the second terms of the right-hand side of eq II are $A + C$ and $-A$, respectively. The laser fluences at 248 and 762 nm were adjusted to produce comparable $O(^3P)$ concentrations and, thus, minimize any errors arising from a small nonlinearity in the variation of the resonance fluorescence signal with $O(^3P)$ concentration.

The excitation efficiency was determined at various ozone concentrations and laser fluences to be, on the average 35% ± 5% of the calculated excitation efficiency (given in the Appendix A). The difference between the measured and calculated excitation efficiency could be due to uncertainties in measured laser fluence, line width of the laser, and errors in the calculated efficiency (for example, due to the line shapes being different from what we assumed). Since these experiments were completed, we discovered that the output of the 762 nm dye laser contained a significant amount of "super radiance," that is, light due to spontaneous emission of the dye that was spread over a very large wavelength range and accounted for at least

TABLE 2: Summary of Experimental Conditions and the Rate Coefficients for the Reaction of $O_2(^1\Sigma)$ with H_2

T (K)	P (Torr)	$[O_2]$ (10^{17} molecule cm^{-3})	$[H_2]$ range (10^{15} molecule cm^{-3})	$[O_3]$ (10^{13} molecule cm^{-3})	flow velocity (cm s^{-1})	$[O_2(^1\Sigma)]$ (10^{11} molecule cm^{-3})	$k \pm 2\sigma$ (10^{-13} cm^3 molecule^{-1} s^{-1})	rotational level pumped	laser energy at 762 nm (mJ pulse^{-1})
209	18	2.6	1−14	10.4−11.4	12	10−20	4.52 ± 0.39	R9Q10	6−12
230	18	2.3	1−14	11.3	14	9−13	4.97 ± 0.30	R9Q10	4−12
248	18	2.2	1−13	10	15	5−17	6.47 ± 0.43	R9Q10	4−12
271	18	2	2−12	9	16	8−11	7.56 ± 0.38	R9Q10, P5P5	5−12
298	18−70	1.0−4.2	1−15	8−11	10−20	5−10	9.31 ± 0.30	R9Q10, P5P5, R13Q14	4−12
323	18	1.6	1.8−11	6.2	19	4−11	11.6 ± 0.64	R9Q10	5−12
348	18	1.5−1.7	0.6−6.4	6.9−7.4	18	4−9	12.8 ± 0.62	R9Q10	5−12
373	19	1.7	0.6−6.4	6	21	6−11	13.95 ± 0.35	R9Q10	13−27

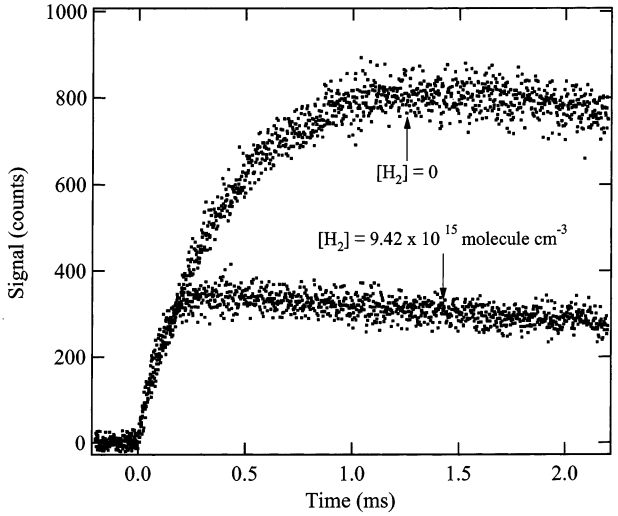

Figure 3. Temporal profiles of $O(^3P)$ following excitation of O_2 at 762 nm in the presence of O_3 with ($[H_2] = 9.4 \times 10^{15}$ molecule cm^{-3}) and without ($[H_2] = 0.0$ molecule cm^{-3}) hydrogen.

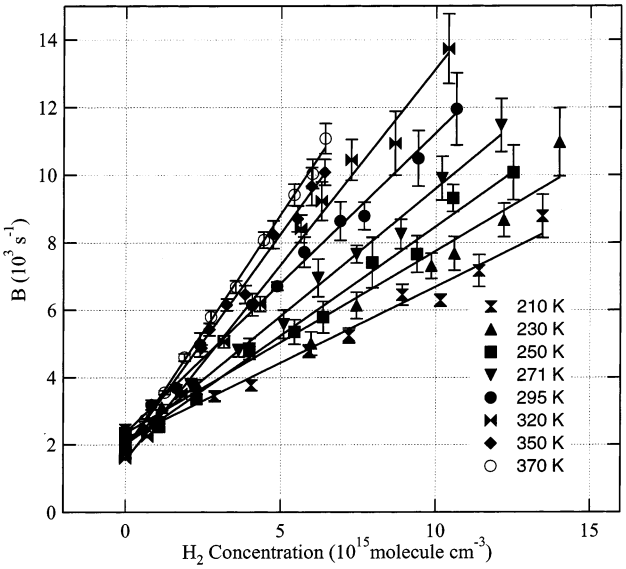

Figure 4. Plots of B values (first-order production rate coefficient for the removal of $O_2(^1\Sigma)$) as a function of $[H_2]$ at different temperatures indicated. The slopes of the plots yield the rate coefficients for the reaction of $O_2(^1\Sigma)$ with H_2 at those temperatures.

part of the difference. Therefore, we used the experimentally measured excitation probability to obtain conservative upper limits for OH yield in reaction 1.

2. Rate Coefficient of $O_2(^1\Sigma_g) + H_2$ Reaction. We measured the total rate coefficient for reaction 1, that is, loss of $O_2(^1\Sigma)$, as described earlier. The $[O_3]$ was monitored constantly and maintained at a constant known level. All measurements were made under pseudo-first-order conditions in $O_2(^1\Sigma)$ (i.e., $[O_2(^1\Sigma)]_0 \ll [H_2]$); $[O_2(^1\Sigma)]_0$ was less than 10^{12} molecule cm^{-3} such that the maximum $[O(^3P)]$ was also less than 10^{12} molecule cm^{-3}. The $O(^3P)$ signal was observed to deviate slightly from a linear signal−concentration relationship when $[O(^3P)]$ was greater than 2×10^{12} molecule cm^{-3}, presumably due to absorption of VUV atomic radiation (both coming in to the reaction volume from the lamp and going out of the reaction volume to the PMT).

Temporal profiles of $O(^3P)$ in the 762 nm excitation of a mixture of O_2 and O_3 in the absence and the presence of H_2 are shown in Figure 3. Such profiles were fit to eq IV in which A and B parameters are given by

$$A = -k_{6a}[O_3][O_2(^1\Sigma)]_0/(k_1[H_2] + k_6[O_3] + k_7 - k_8) \quad \text{(VIII)}$$

$$B = (k_1[H_2] + k_6[O_3] + k_7) \quad \text{(IX)}$$

Figure 4 shows a plot of the obtained B parameter (eq IX), the first-order rate coefficient for the loss of $O_2(^1\Sigma)$, as a function of $[H_2]$ at different temperatures. The intercepts of these plots are the first-order rate coefficients for the loss of $O_2(^1\Sigma)$ via reaction 3 and any other loss for $O_2(^1\Sigma)$ assumed to be first-order in its concentration. The slopes of the plots are k_1, the rate coefficients for the loss of $O_2(^1\Sigma)$ by H_2 at different temperatures. The measured values of k_1 between 209 and 373 K are listed in Table 2.

The Arrhenius plot of k_1 (on a logarithmic scale) versus $1/T$ is shown in Figure 5. A fit of $\ln(k_1)$ versus $1/T$ to a straight line yielded

$$k_1(T) = (6.8 \pm 1.2) \times 10^{-12} \exp[-(590 \pm 52)/T] \text{ cm}^3 \text{ molecule}^{-1} \text{ s}^{-1} \quad \text{(X)}$$

where the uncertainties are 2σ and $\sigma_A = A\sigma_{\ln A}$ obtained in the linear least-squares fit.

We measured k_1 by preparing $O_2(^1\Sigma, v = 0)$ in different rotational states to check for any dependence on the rotational excitation. The measured rate coefficients were independent of the rotational excitation and laser pulse energies (see Table 2). Rapid rotational relaxation of $O_2(^1\Sigma)$ (compared to its electronic quenching by or reaction with H_2) helped maintain a thermal rotational distribution during the course of reaction 1.

The main source of systematic error in our measurements was the accuracy of the concentration of H_2, which was estimated to be less than 5% at the 95% confidence limit. The nonlinear least-squares analysis of the temporal profile of $O(^3P)$ introduced error in determining the values of various parameters, $A-D$ (eq IV). This error was estimated to be ∼7%, which was the standard deviation of the precision of the fitting. We estimate the total error to be ∼15% at the 95% confidence level.

Previous determinations of k_1 at 298 K and the Arrhenius parameters for k_1, where available, are given in Table 3. The lowest values of k_1(298 K) are associated with the studies in

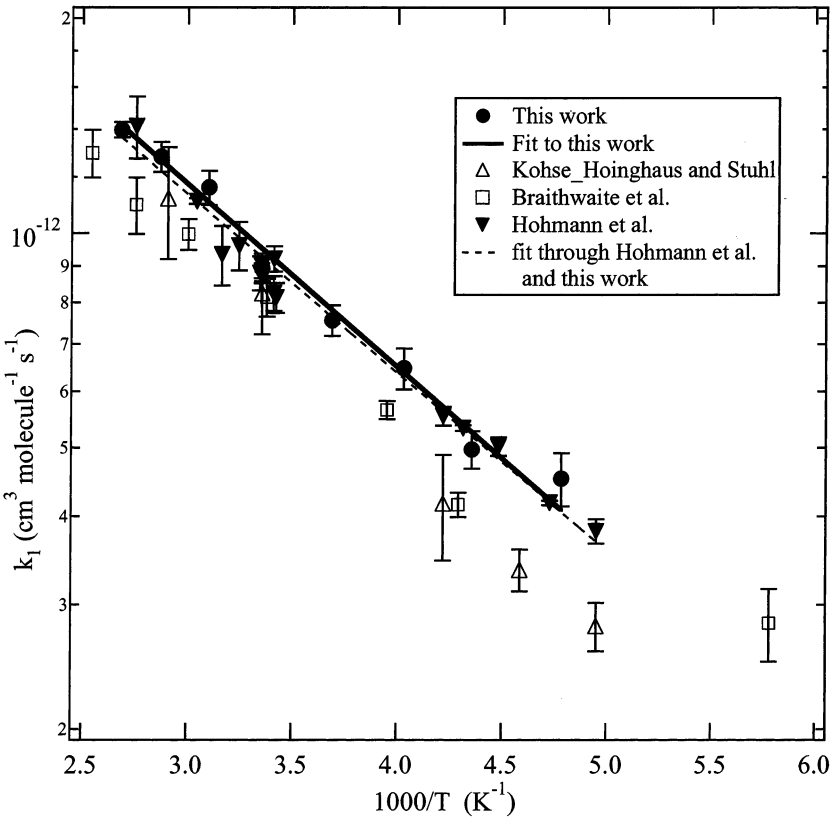

Figure 5. Plots of the second-order rate coefficients, k_1, on a logarithmic scale, as a function of $1/T$. The data obtained by previous investigators (various symbols shown in the figure) are also included.

TABLE 3: A Comparison of Our Measured Values of k_1 and Its Arrhenius Parameters with Those from Previous Studies[a]

T range (K)	$O_2(^1\Sigma)]_0$ (molecule cm^{-3})	P (Torr)	$k_1(298)$[b]	A[c]	E (cal mol^{-1})	source of $O_2(^1\Sigma)$	ref
202−344	1×10^{10}	71−77 (He buffer gas)	8.2 ± 1.0	$8.0^{+3.1}_{-2.3}$	1364 ± 145	O_2/H_2 VUV laser photolysis/O_2	5
173−393	$(3-12) \times 10^{12}$	5 (O_2 buffer gas)	8.2 ± 0.5	5.2 ± 0.6	1100	O_3/266 nm/O_2	3
298	3×10^8	1−5	7.0 ± 0.3			discharge flow	7
298	2×10^{12}	1−3	4.5 ± 2.0			discharge + energy pooling self-reaction of $O_2(^1\Delta)$	9
295 ± 5	$(3-30) \times 10^{12}$	10−100	6.1 ± 0.9			pulsed laser excitation by tunable 762 nm	10
298	1×10^{10}	1−5	7.1 ± 0.1			discharge flow	8
210−350	$<1 \times 10^{10}$	70−80	9.2 ± 1.0	6.3 ± 0.5	1137 ± 40	O_2/H_2 VUV laser photolysis/O_2	12
292 and 500−1000		6	4.67 ± 0.17 at 292 K			discharge + energy pooling self-reaction of $O_2(^1\Delta)$	11
209−373	$(4-20) \times 10^{11}$	18−70	9.3 ± 0.6	6.8 ± 1.2	1168 ± 103	pulsed laser excitation by tunable 762 nm	this work

[a] All previous studies used 762 nm fluorescence for the detection of $O_2(^1\Sigma)$. [b] Units of $k_1(298)$ are 10^{-13} cm^3 molecule^{-1} s^{-1}. [c] Units of A are 10^{-12} cm^3 molecule^{-1} s^{-1}.

which $O_2(^1\Sigma)$ was generated via the energy pooling reaction of $O_2(^1\Delta)$ with itself. It is possible that $O_2(^1\Sigma)$ was regenerated in such systems from $O_2(^1\Delta)$, which was likely produced via the quenching of $O_2(^1\Sigma)$ by H_2 and (or) the recombination of $O(^3P)$ atoms to give $O_2(^1\Sigma)$ followed by its conversion to $O_2(^1\Delta)$.[7] If we ignore the k_1 values from the studies in which $O_2(^1\Sigma)$ was generated via the energy pooling reaction, the measured values range between 6.1×10^{-13} and 9.3×10^{-13} cm^3 molecule^{-1} s^{-1} with an average value around 7.9×10^{-13} cm^3 molecule^{-1} s^{-1}, which is somewhat lower than our measured value.

k_1 has been measured as a function of temperature by three groups, Kohse-Hoinghauas and Stuhl,[5] Braithwaite et al.,[3] and Hohmann et al.[12] These results are also plotted in Figure 5 along with our data for comparison. Clearly our data are in good agreement with the most recent previous study of Hohmann et al. The data of Braithwaite et al.[3] and of Kohse-Hoinghauas and Stuhl[5] are consistently lower than both our data and those of Hohmann et al. The difference between the later two studies has been attributed to the impurities present in the system of Kohse-Hoinghauas and Stuhl.[5] The reasons for the discrepancy between the data of Braithwaite et al.[3] and ours are not apparent. Assuming that the results of Kohse-Hoinghauas and Stuhl[5] are superseded by the work of Hohmann et al.[12] from the same group, we can fit our data and that of Hohmann et al.[12] to derive a value for atmospheric purposes.

$$k_1(T) = (6.4 \pm 0.8) \times 10^{-12} \exp[-(577 \pm 35)/T] \text{ cm}^3 \text{ molecule}^{-1} \text{ s}^{-1} \quad \text{(XI)}$$

This is very close to the value of Hohmann et al. because they have measured k_1 at two times as many temperatures as we have.

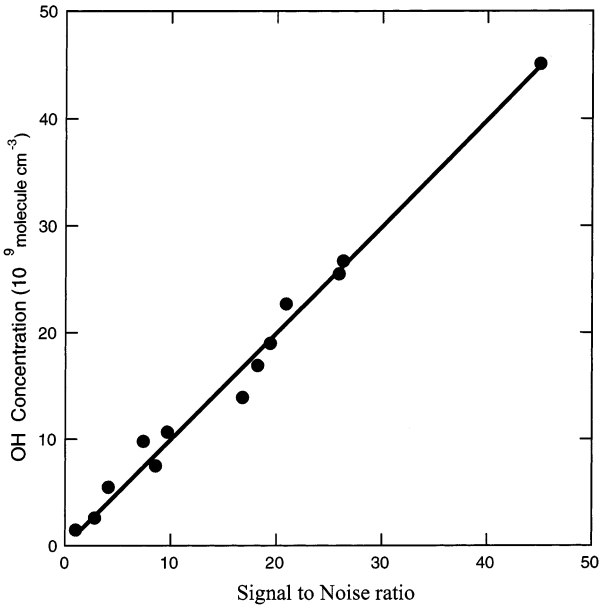

Figure 6. A plot of the calculated OH concentration against the measured signal-to-noise ratio. The standard deviation of the background averaged from 200 laser shots gave the noise level. The average of the LIF signal from 200 shots using the 248-nm photolysis is the signal.

3. OH Detection: Upper Limit of OH Yield in Reaction 1. The OH detection sensitivity was determined by creating a known (calculated) concentration of OH under the conditions of the experiments used to look for OH in reaction 1 and measuring the laser-induced fluorescence signal. For this purpose, we could use the same gas mixture used in searching for OH production in reaction 1 but photolyze it with 248-nm radiation instead of 762-nm light.

(a) OH Signal Calibration. We first determined the detection sensitivity for OH to derive an upper limit for the OH yield from reaction 1. A small quantifiable portion of the photolytically produced $O(^1D)$ reacted with H_2 to give OH. The majority of $O(^1D)$ was quenched by O_2 to produce $O_2(^1\Sigma)$ and $O(^3P)$. The ozone concentration was maintained in the range $(8-10) \times 10^{13}$ molecule cm^{-3}. The 248-nm laser energy fluence was in the range of 0.9 to 6 mJ cm^{-2}. Experiments were performed at a constant pressure of about 150 Torr of O_2. The H_2 concentration was varied between 2×10^{15} and 47×10^{15} molecule cm^{-3}. The $[OH]_0$ was calculated from the known O_3 absorption cross section at 248 nm, the laser fluence, $[O_3]$, $[O_2]$, and $[H_2]$, and the rate coefficients for their reactions with $O(^1D)$.[19] The uncertainty in the calculated OH concentration, attributed to the uncertainties in the involved rate coefficients and concentrations, was ~25%. Uncertainties in all other quantities such as laser fluence, quantum yields for $O(^1D)$ production, and absorption cross sections of O_3 do not introduce additional uncertainties in the OH yield because they are also involved in the calculation of $[O_2(^1\Sigma)]_0$ and hence cancel out.

Various concentrations of OH were produced, and the measured S/N was plotted as a function of the calculated concentration (Figure 6). The slope of the plot, which is the measurable OH concentration for a S/N ratio of unity, is $(9.8 \pm 0.3) \times 10^8$ molecule cm^{-3}. We take the detection limit for OH as 1.0×10^9 molecule cm^{-3} for a signal-to-noise ratio of unity for determining the upper limit of OH production in reaction 1. Photolysis of a known concentration of H_2O_2 at 248 nm in 155 Torr of O_2 also gave a detection sensitivity of $\sim 1 \times 10^9$ molecule cm^{-3}.

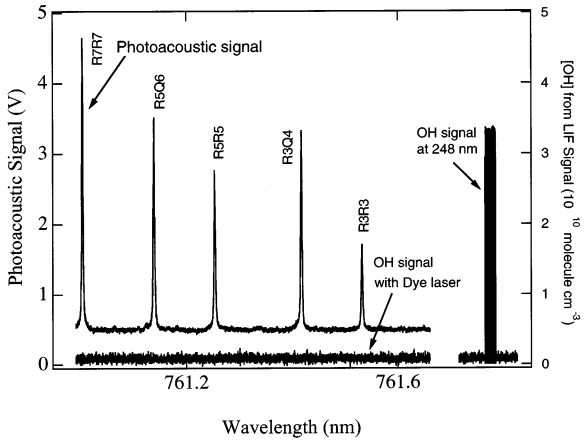

Figure 7. Plots of the photoacoustic signal and the OH signal as a function of wavelength of the dye laser around 761 nm. These data represent a very small wavelength window over which the laser was scanned. OH signal from the calibration experiment is shown at the right. Clearly, the OH signals, when $O_2(^1\Sigma)$ was generated, as shown by the photoacoustic signal, are essentially zero.

(b) OH Yield in Reaction 1. We employed two methods to determine the upper limits of OH production in reaction 1. In the first set of measurements, $O_2(^1\Sigma)$ was generated by direct excitation of O_2 near 762 nm. Figure 7 shows the OH signal as a function of wavelength around 761 nm at 298 K for an O_2 pressure of 155 Torr. The calibration signal with 248-nm photolysis of ozone is shown at right. The photoacoustic signal from this scan is also included in the figure. Clearly, we do not see any OH signal when 5×10^{13} molecule cm^{-3} of $[O_2(^1\Sigma)]_0$ was generated by excitation with 21 mJ of 761.003 nm, R(7)R(7) line of O_2. A 100% yield of OH from reaction 1 would have given $[OH]_0 = 1 \times 10^{14}$ molecule cm^{-3}. Because our detection limit for OH is 1×10^9 molecule cm^{-3}, we calculate an upper limit to the OH yield of $\Phi_{1b} \approx 10^{-5}$. Including the uncertainties in measuring laser fluence, the efficiency of the excitation of O_2 by 762 nm, we assign a conservative upper limit as 4×10^{-5}.

Focusing the 762-nm laser beam inside the reactor, which increased the fluence by a factor of 10 but did not change the total pulse energy, also produced no detectable OH−LIF signal. Preparation of $O_2(^1\Sigma)$ in various rotational states up to $J = 15$ also did not result in any measurable OH−LIF signal. It is likely that rotational thermalization of the excited O_2 is much faster than total $O_2(^1\Sigma)$ loss rate under these experimental conditions.

An alternative method was also used to place a limit on the OH yield. In this case a mixture of O_3, O_2, and H_2 were photolyzed at 248 nm. The temporal profiles of OH were measured for different H_2 concentrations. One such profile is shown in Figure 8. Using the reactions listed in Table 1, we calculated the temporal profiles of OH concentrations with varying values of k_{1b}, and an example is shown in Figure 8. Clearly, the OH production in reaction 1 is very small. On the basis of the perceived detection in the curvature due to reaction 1b, we place an upper limit of $k_{1b} \leq 5 \times 10^{-16}$ cm^3 molecule^{-1} s^{-1}. Such limits were obtained for different concentrations of ozone and H_2 at various photolysis laser fluences. From such analyses, we determined the upper limit at 298 K to be $k_{1b} \leq 5 \times 10^{-16}$ cm^3 molecule^{-1} s^{-1}, giving an upper limit for the yield of channel 1b of $\Phi_{1b} \leq 6 \times 10^{-4}$.

It should be noted that the $O_2(^1\Sigma)$ produced by interaction of $O(^1D)$ with O_2 could be in $v'' = 0$ and 1 states. However, the rate coefficient for the vibrational relaxation of $O_2(^1\Sigma, v = 1)$

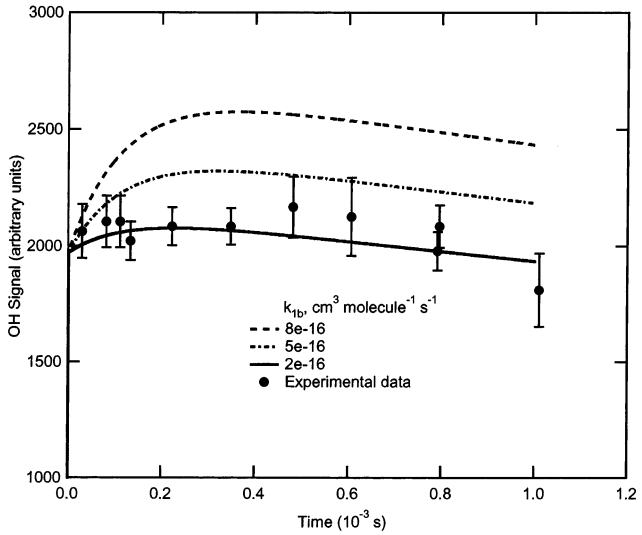

Figure 8. Temporal profile of OH signal in the photolysis of $O_3/H_2/O_2$ at 248 nm. The three curves were simulated using the values of k_{1b} shown in the figure. Clearly, the value of k_{1b} is less than 5×10^{-16} cm^3 molecule^{-1} s^{-1}.

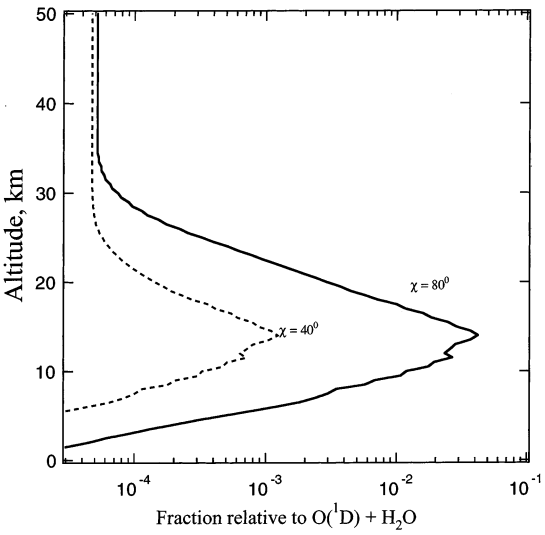

Figure 9. Calculated ratio of OH production from reaction 1 relative to reaction of O(^{1}D) with H_2O at two different zenith angles (40° and 80°) as a function of altitude for $\Phi_{1b} = 4 \times 10^{-5}$ at solar zenith angle of 40° (dashed line) and 80° (solid line).

by ground-state oxygen, $O_2(^3\Sigma)$, is 2.2×10^{-11} cm^3 molecule^{-1} s^{-1}. Hence, in our experiments, $O_2(^1\Sigma)$ would be in $v = 0$ during its removal by H_2.

Clearly, the first method is better suited for measuring the upper limit for k_{1b}. The second method, though not as precise, substantiated the conclusion of the first method. To check whether k_{1b}/k_1 varied with temperature, we measured k_{1b} at 209 K by the first method. The obtained upper limit of 1×10^{-5} for Φ_{1b} at 209 K clearly shows that OH production in reaction 1 is not important at lower temperatures.

Atmospheric Modeling. We used a 1-D model to quantify the importance of reaction 1b compared to reaction 13

$$O(^1D) + H_2O \rightarrow 2OH \qquad (13)$$

for OH production in the troposphere and stratosphere. Temperature and pressure, as well as the abundance of N_2, O_2, H_2O (midlatitude mean from Standard Atmosphere, 1976), CO_2 (360 ppmv), O_3 (350 DU, profile from Standard Atmosphere, 1976),[20] and H_2 (Brasseur and Solomon, 1986)[21] were prescribed in the model. Steady-state mixing ratios of $O(^1D)$ and $O_2(^1\Sigma)$ were calculated. $O(^1D)$ was produced from O_3 photolysis and was lost via quenching by N_2 and O_2 and by reaction with H_2O. Photolysis rates of O_3 for $O(^1D)$ production were calculated using a two-stream δ-Eddington multiple scattering calculation based on Toon et al.[22] $O_2(^1\Sigma)$ was produced by absorption of radiation by $O_2(^3\Sigma)$ between 759 and 775 nm, as well as from the reaction of $O(^1D)$ with $O_2(^3\Sigma)$. The values for the radiative excitation rate of $O_2(^3\Sigma)$ in the wavelength range 759−775 were taken from Mlynczak.[23] Removal via quenching by N_2, H_2O, CO_2, O_3, O_2, and H_2 and by spontaneous emission was included. All rate coefficients, except those determined in this study, were taken from DeMore et al.[19] In addition, the Einstein coefficient for $O_2(^1\Sigma)$ spontaneous emission to $O_2(^3\Sigma)$ was taken to be 0.085 s^{-1},[24−26] and the rate constant for the reaction of $O_2(^1\Sigma)$ with H_2 was taken to be $6.8 \times 10^{-12} \exp(-590/T)$ cm^3 molecule^{-1} s^{-1} (this work). All of our calculations were performed using an upper limit of $k_{1b} = (4 \times 10^{-5})k_1(T)$.

The production of $O_2(^1\Sigma)$ is dominated by reaction 4 in the middle and upper stratosphere, but solar absorption dominates in the tropopause region where both Toumi[1] and Siskind et al.[2] have suggested a large role for reaction 1 in OH production. Among the various loss processes, the quenching by H_2O is the dominant loss mechanism for $O_2(^1\Sigma)$ in the lower troposphere with N_2 and CO_2 playing important roles throughout the troposphere and stratosphere and O_3 becoming important in the middle and upper stratosphere. Figure 9 shows the ratio of the calculated maximum OH production via reaction 1b relative to the well-established $O(^1D) + H_2O$ (reaction 13) source as a function of altitude for two different zenith angles. When our upper limit for the yield of channel 1b is used, it is clear that reaction 1 contributes no more than 10% of the total OH production rate at the tropopause at large zenith angles (80°). At lower solar zenith angles and other altitudes, reaction 1b cannot play a major role in OH production.

In the troposphere, most of the $O_2(^1\Sigma)$ is produced by absorption of solar radiation and does not depend on O_3 concentration. So, if O_3 were lower, the $O(^1D)$ production and hence OH from this channel would be lower; under such conditions, $O_2(^1\Sigma)$ could contribute more to OH production. However, the integrated OH produced in a summer day by reaction 1 is much smaller than the $O(^1D) + H_2O$ source. Also, in regions such as the upper troposphere, there are other possible sources of OH.[27−30] Therefore, it appears that the role played by reaction 1b in producing OH is small in the upper atmosphere.

In the upper region of the atmosphere (i.e., stratosphere and above), most $O_2(^1\Sigma)$ is produced by reaction 4, and therefore, the ratio of $[H_2O]$ to $[H_2]$ determines the relative contribution of reaction 1 to OH production. Here again, the contribution of reaction 1 is small because $[H_2O]$ is greater than $[H_2]$ and the ratio of the rate coefficients, k_{13}/k_{1b}, is much larger than unity. Thus, the absolute [OH] from the title reaction is small.

The results of Toumi[1] and Siskind et al.[2] suggested a significant production of OH from reaction 1 relative to reaction 13 in the 10−15 km range of altitude if the OH yield was of the order of 1% or so. Toumi did not include the quenching of $O_2(^1\Sigma)$ by H_2O, which is the dominant removal mechanism up to 10 km and, thus, obtained a larger OH production rate from reaction 1b. Toumi also used the 298 K value of k_1 instead of the temperature-dependent values used by Siskind et al. and by us. Thus, even though Toumi and Siskind et al. highlighted the

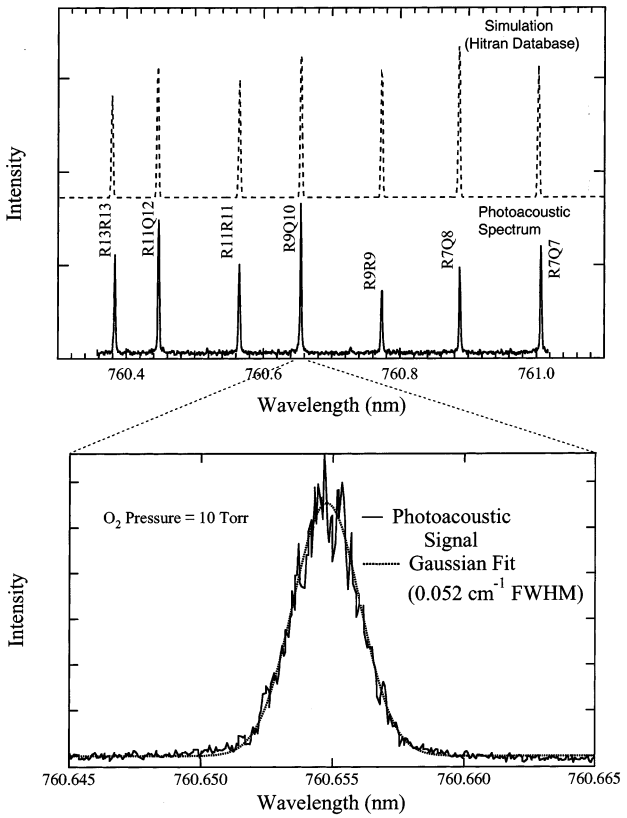

Figure A1. The upper panel shows the photoacoustic spectra of O_2 along with O_2 lines from Hitran database. Lower panel shows that the convolved simulated line shape is Gaussian at low pressure of O_2 (10 Torr). The experimental spectrum was slightly shifted to match the simulated spectrum. The two were compared to obtain the laser line width.

possible importance of this reaction, our determination of very low yield for OH in reaction 1 shows that this reaction can be neglected in the Earth's atmosphere.

Acknowledgment. This work was funded partially by NOAA's Climate and Global Change research program. We thank Prof. F. Stuhl for providing the data plotted in Hohmann et al.[12]

Appendix A

Excitation Probability in the Direct O_2 Excitation near 762 nm. A portion of the photoacoustic spectrum of O_2 is shown in Figure A1 along with a calculated spectrum using relative intensities and line positions from the Hitran database. The line assignments are from the Hitran database. To determine the line width of the etalon-narrowed 762-nm dye-laser beam, we measured the width of O_2 photoacoustic transitions at 10 Torr and 298 K, where the pressure broadening is negligible (0.001 cm^{-1} fwhm). The Doppler width at this temperature is 0.030 cm^{-1}, assuming a Gaussian profile. The observed photoacoustic transition was fit to a Gaussian with a width of 0.052 cm^{-1} as shown in the lower panel of Figure A1. The dye-laser line can thus be inferred to have a Gaussian shape with a width of 0.043 cm^{-1}. Using this line width, we can calculate the efficiency of the direct excitation at various O_2 pressures inside the reactor. The Doppler and pressure-broadened profiles of appropriate widths were convolved, normalized to the integrated line intensity (cm^2 $molecule^{-1}$ cm^{-1}) from the Hitran database[31] to generate a pressure- and temperature-dependent Voigt profile.

TABLE A1: Excitation Probability of O_2 in the RF Cell at Different Temperatures

line intensity (10^{-24} cm^2 cm^{-1})	T (K)	P (Torr)	excitation probability (10^{-7} mJ^{-1} cm^{-2})
Line Wavelength R9Q10, 760.654 65 nm			
9.43	209	5.6	6.77
9.30	230	5.4	6.65
9.14	248	5.6	6.44
8.91	271	5.6	6.21
8.64	298	6.1	5.95
8.35	323	5.6	5.68
8.06	348	5.2	5.43
7.78	373	6.6	5.17
Line Wavelength R13Q14, 760.258 44 nm			
6.30	298	6.2	4.33
Line Wavelength P5P5 at 763.032 27 nm			
8.16	271	6.8	5.23

(Because we used the Hitran software to generate the intensity for a given rotational line, the temperature dependence was automatically included.[31]) The Gaussian laser line profile was normalized to the measured laser fluence, multiplied by the Voigt profile at the same center frequency, and integrated to give the excitation probability, P_E. The concentration of $O_2(^1\Sigma_g)$ produced by laser excitation is given by

$$[O_2(^1\Sigma_g)]_0 = P_E[O_2(^3\Sigma)] \qquad \text{(IA)}$$

Table A1 lists the excitation probability for a few transitions at different temperatures for 1 mJ cm^{-2} $pulse^{-1}$ of laser fluence.

The collisional self-broadening coefficient for $O_2(b^1\Sigma \leftarrow X^3\Sigma)$ lines has been recently measured to be 1.25×10^{-4} by Angelis et al.[32] and 7×10^{-5} cm^{-1} $Torr^{-1}$ by Pope et al.[33] We also measured this coefficient from the variation of the apparent O_2 line widths in our system at O_2 pressure from 10 to 1000 Torr. Our value of $(1.00 \pm 0.25) \times 10^{-4}$ cm^{-1} $Torr^{-1}$ (where error is 2σ precision) is in accord with the previous measurements.[32,33] It should be noted that convolution of laser line width with Doppler broadening yielded fwhm comparable to the pressure broadening at ~400 Torr. Because our highest pressure was 1000 Torr of O_2 and the laser line width was 0.043 cm^{-1}, this method was not as sensitive to line broadening as the recent measurements of Angelis et al.[32] in which the laser line width (fwhm = 0.0017 cm^{-1}) was much smaller than the width of the absorption line.

References and Notes

(1) Toumi, R. *Geophys. Res. Lett.* **1993**, *20*, 25.
(2) Siskind, D. E.; Summers, M. E.; Mlynczak, M. G. *Geophys. Res. Lett.* **1993**, *20*, 2047.
(3) Braithwaite, M.; Ogryzlo, E. A.; Davidson, J. A.; Schiff, H. I. *J. Chem. Soc., Faraday Trans. 2* **1976**, *72*, 2075.
(4) Filseth, S. V.; Zia, A.; Welge, K. H. *J. Chem. Phys.* **1970**, *52*, 5502.
(5) Kohse-Hoinghauas, K.; Stuhl, F. *J. Chem. Phys.* **1980**, *72*, 3720.
(6) Dunlea, E. J. Atmospheric Reactions of Electronically Excited Atomic and Molecular Oxygen. Ph.D. Thesis, University of Colorado, Boulder, CO, 2002.
(7) Choo, K. Y.; Leu, M.-T. *Int. J. Chem. Kinet.* **1985**, *17*, 1155.
(8) Michelangeli, D. V.; Choo, K.-Y.; Leu, M.-T. *Int. J. Chem. Kinet.* **1988**, *20*, 915.
(9) Singh, J. P.; Setser, D. W. *J. Phys. Chem.* **1985**, *89*, 5353.
(10) Wildt, J.; Bednarek, G.; Fink, E. H.; Wayne, R. P. *Chem. Phys.* **1988**, *122*, 463.
(11) Borrell, P.; Richards, D. S. *J. Chem. Soc., Faraday Trans. 2* **1989**, *85*, 1401.
(12) Hohmann, J.; Muller, G.; Schonnenbeck, G.; Stuhl, F. *Chem. Phys. Lett.* **1994**, *217*, 577.
(13) Turnipseed, A. A.; Vaghjiani, G. L.; Gierczak, T.; Thomson, J. E.; Ravishankara, A. R. *J. Chem. Phys.* **1991**, *95*, 3244.

(14) Vaghjiani, G. L.; Ravishankara, A. R. *J. Chem. Phys.* **1990**, *92*, 996.
(15) Talukdar, R. K.; Burkholder, J. B.; Schmoltner, A.-M.; Roberts, J. M.; Wilson, R.; Ravishankara, A. R. *J. Geophys. Res.* **1995**, *100*, 14163.
(16) Vaghjiani, G. L.; Ravishankara, A. R. *J. Phys. Chem.* **1989**, *93*, 1948.
(17) Brion, J.; Chakir, A.; Charbonnier, J.; Daumont, D.; Parisse, C.; Malicet, J. *J. Atmos. Chem.* **1998**, *30*, 291.
(18) Burkholder, J. B.; Talukdar, R. K. *Geophys. Res. Lett.* **1994**, *21*, 581.
(19) DeMore, W. B.; Sander, S. P.; Golden, D. M.; Hampson, R. F.; Kurylo, M. J.; Howard, C. J.; Ravishankara, A. R.; Kolb, C. E.; Molina, M. J. *Chemical Kinetics and Photochemical Data for Use in Stratospheric Modeling*; Evaluation Number 12; Jet Propulsion Laboratory: 1997.
(20) United States National Oceanic and Atmospheric Administration. *U. S. Standard Atmosphere*; U.S. Government Printing Office: Washington, DC, 1976.
(21) Brasseur, G.; Solomon, S. *Aeronomy of the Middle Atmosphere*, 2nd ed.; D. Reidel Publishing Company: Dordrecht, Netherlands, 1986.
(22) Toon, O. B.; McKay, C. P.; Ackerman, T. P.; Santhanam, K. *J. Geophys. Res.* **1989**, *94*, 16287.
(23) Mlynczak, M. G. *Geophys. Res. Lett.* **1993**, *20*, 1439.
(24) Klotz, R.; Marian, C. M.; Peyerimhoff, S. D.; Hess, B. A.; Bunker, R. J. *Chem. Phys.* **1984**, *89*, 223.
(25) Long, C.; Kearns, D. R. *J. Chem. Phys.* **1973**, *59*, 5729.
(26) Wayne, R. P. Reactions of Singlet Molecular Oxygen in the Gas Phase. In *Singlet* O_2; Frimer, A. A., Ed.; CRC Press: Boca Raton, FL, 1985; Vol. 1; p 81.
(27) Brune, W. H.; Faloona, I. C.; Tan, D.; Weinheimer, A. J.; Campos, T.; Ridely, B. A.; Vay, S. A.; Collins, J. E.; Sachse, G. W.; Jaegle, L.; Jacob, D. J. *Geophys. Res. Lett.* **1998**, *25*, 1701.
(28) Crawford, J.; Davis, D.; Olson, J.; Chen, G.; Liu, S.; Gregory, G.; Barrick, J.; Sachse, G.; Sandholm, S.; Heikes, B.; Singh, H.; Blake, D. *J. Geophys. Res.* **1999**, *104*, 16255.
(29) Jaegle, L.; Jacob, D. J.; Wennberg, P. O.; Spivakovsky, C. M.; Hanisco, T. F.; Lanzendorf, E. J.; Hintsa, E. J.; Fahey, D. W.; Keim, E. R.; Proffitt, M. H.; Atlas, E. L.; Flocke, F.; Schauffler, S.; McElroy, C. T.; Midwinter, C.; Pfister, L.; Wilson, J. C. *Geophys. Res. Lett.* **1997**, *24*, 3181.
(30) McKeen, S. A.; Gierczak, T.; Burkholder, J. B.; Wennberg, P. O.; Hanisco, T. F.; Keim, E. R.; Gao, R. S.; Liu, S. C.; Ravishankara, A. R.; Fahey, D. W. *Geophys. Res. Lett.* **1997**, *24*, 3177.
(31) Rothman, L. S.; Rinsland, C. P.; Goldman, A.; Massie, S. T.; Edwards, D. P.; Flaud, J.-M.; Perrin, A.; Camy-Peyret, C.; Dana, V.; Mandin, J.-Y.; Schroeder, J.; McCann, A.; Gamache, R. R.; Watson, R. B.; Yoshino, K.; Chance, K. V.; Jucks, K. W.; Brown, L. R.; Nemtchinov, V.; Varanasi, R. *J. Quant. Spectrosc. Radiat. Transfer* **1998**, *60*, 665.
(32) Angelis, M. D.; Gianfrani, L.; Pavone, F.; Sasso, A.; Tino, G. M. *IL Nuovo Cimento* **1996**, *18D*, 557.
(33) Pope, R. S.; Wolf, P. J.; Perram, G. P. *J. Quant. Spectrosc. Radiat. Transfer* **2000**, *64*, 363.